Hybrid chemo-biocatalysts prepared in one step from zeolite nanocrystals and enzyme-polyelectrolyte complexes

*Margot Van der Verren, Valentin Smeets, Aurélien vander Straeten, Christine C. Dupont-Gillain, Damien P. Debecker**

Institute of Condensed Matter and Nanosciences (IMCN), Université catholique de Louvain (UCLouvain) *e-mail : damien.debecker@uclouvain.be

KEYWORDS

Hybrid catalysis; spray drying; chemo-enzymatic cascade reaction; aerosol process; protein-polyelectrolyte complexes; biocatalysis; Glucose oxidase; TS-1 zeolite

ABSTRACT

The combination of heterogeneous catalysts and enzymes, in so-called hybrid catalysts, is an attractive strategy to effectively run chemoenzymatic reactions. Yet, the preparation of such bifunctional materials remains challenging because both the inorganic and the biological moieties must be integrated in the same solid, while preserving their intrinsic activity. Combining an enzyme and a zeolite, for example, is complicated because the pores of the zeolite are too small to accommodate the enzyme and a covalent anchorage on the surface is often ineffective. Herein, we developed a new pathway to prepare a hybrid catalyst built from glucose oxidase and TS-1 zeolite. Such hybrid material can catalyze the in situ formation of H_2O_2, which is subsequently used by the zeolite to trigger the epoxidation of allylic alcohol. Starting from an enzymatic solution and a suspension of zeolite nanocrystals, the hybrid catalyst is obtained in one step, using a continuous spray drying method. While enzymes are expectedly unable to resist the conditions used in spray drying (temperature, shear stress, etc.), we leverage on the preparation of "enzyme-polyelectrolyte complexes" (EPCs) to increase the enzyme stability. Importantly, the use of EPCs also appears to prevent enzyme leaching and to stabilize the enzyme against pH changes. We show that the one-pot preparation by spray drying gives access to hybrid catalysts with unprecedented performance in the targeted chemoenzymatic reaction. Interestingly, the hybrid catalyst performs much better than the two catalysts operating as separate entities. We anticipate that this strategy could be used as an adaptable method to prepare other types of multifunctional materials.

Introduction

Targeting the development of more sustainable processes, researchers continuously explore new synthesis pathways for producing chemicals under milder conditions while limiting the formation of polluting and hazardous substances (1). In this context, catalysis is known to play a central role (2). As "the 9th principle of green chemistry" (3), catalysis allows inventing more efficient chemical routes for the production of chemicals, evolving towards intensified processes, and simplifying industrial workup procedures (4). While catalysis science is classically compartmented into three sub-fields – homogeneous, heterogeneous and enzymatic catalysis – it nowadays appears essential to harness the strengths of different types of catalysts to design greener chemical processes (5).

On the one hand, heterogeneous catalysts are considered as robust catalysts with moderate intrinsic performance (selectivity, yield) but large scope of application. On the other hand, biocatalysis is a highly appealing method to produce chemicals under mild conditions and therefore, with a low environmental impact, while achieving high (enantio)-selectivity and (enantio)-specificity (6). Microbial enzymes are currently widely used at industrial scale. Aminopeptidases and lipases are for example involved in food industry, and particularly in the dairy market (7–9). Several recent reviews have highlighted the industrial interest of microbial enzymes and their various applications (7,10–12). However, the scope of reactions, substrates and conditions remains relatively limited when working with enzymes (13,14).

Combining heterogeneous catalysis with biocatalysis is increasingly envisaged as a solution to leverage on the respective advantages of each partner to effectively run a chemoenzymatic reaction (15–17). In most reported examples, an enzyme and a solid catalyst were used in conjunction, as two distinct entities. Advantageously, the enzyme can be immobilized on a carrier to facilitate recovery and reuse. Even more interestingly, the two catalytic species can be combined in a unique

bifunctional solid (18–20) by immobilizing the enzyme directly onto an active solid catalyst, to form a so-called "hybrid catalyst" (5,21–23). The latter solids are designed to host at least two catalytic active species – a chemical one and an enzymatic one – and to be easily separated from the reaction medium (and potentially reused).

However, working with a hybrid catalyst to run one-pot chemoenzymatic reactions raises several issues. Enzymes are active in mild conditions such as aqueous medium (exclusive of extreme pH values) and ambient temperature, while most inorganic catalysts require relatively harsh conditions (pressure and temperature) and sometimes organic solvents (24,25). But even before envisaging the application of hybrid chemoenzymatic catalysts, their preparation itself represents an important challenge. The successful combination of an enzyme and an inorganic catalyst in a single solid is complicated because this requires to ensure an effective integration of both partners (e.g. by covalent attachment) while preserving the essential properties that confer their activity (i.e. the enzyme tridimensional structure and the peculiar surface chemistry of the solid catalyst). Possible issues associated with the preparation of hybrid catalysts include pore plugging, enzyme leaching, enzyme denaturation, surface poisoning, etc. In fact, only few studies have investigated methods to synthesize true hybrid catalysts (26–29) .

A telling example is the combination of an enzyme with a zeolite catalyst. The latter are ubiquitous in heterogeneous catalysis, including at the industrial scale for biomass upgrading (30), selective oxidation (31), organic synthesis (32), etc. However, their crystalline structure and microporous texture make it complicated to envisage the coupling with an enzyme: the surface usually offers limited anchoring points for covalent attachment and the micropores are too small to host enzymes of a few nanometers. One of the scarce examples found in the literature is the combination of the biocatalytic production of hydrogen peroxide by glucose oxidase (GOx) with

the subsequent oxidation of low olefins to epoxides using titanosilicalite-1 zeolites (TS-1) (21,26,33). TS-1 zeolites feature outstanding catalytic activity in epoxidation at moderate temperature and do not suffer from deactivation in aqueous medium (34–37). In 2010, Vennestrøm et al. proposed the one-pot chemoenzymatic epoxidation of allyl alcohol using the TS-1 zeolite as catalyst and H_2O_2 produced *in situ* by free glucose oxidase (GOx), as the oxidant (26,33). Interestingly, they also disclosed the first example of a true hybrid catalyst for this reaction, having covalently grafted GOx at the surface of TS-1 nanocrystals. However, only traces of epoxide were detected in this case due to a low enzyme loading and poor enzyme stability in the reaction conditions. This can be directly associated with the fact that the TS-1 zeolite – featuring small micropores and a low density of surface hydroxyls – is intrinsically not well suited to host an enzyme.

To overcome these drawbacks, we have recently proposed a two-step strategy for the preparation of an efficient GOx/TS-1 hybrid catalyst (27). First, leveraging on a spray drying technique (38), hollow zeolite microspheres were designed, starting from a suspension of TS-1 nanocrystals. Second, the hollow zeolite microspheres were loaded with GOx and the latter was irreversibly trapped through the formation of aggregates. This is a change in paradigm with respect to the classical approach where the enzyme has to be immobilized onto the surface or into the pore of a solid. The GOx loading could be easily adapted and the enzyme also gained in stability. This original design allowed reaching relatively high levels of epoxide yield in the one-pot chemoenzymatic reaction (27).

Moving further, it is appealing to envisage a more direct procedure to form a GOx/TS-1 hybrid catalyst directly in one step by spray drying of a precursors suspension containing both the zeolite nanocrystals and the enzyme. On the one hand, aerosol processing is well suited for the preparation

of many types of inorganic heterogeneous catalysts (38–46). In fact, aerosol methods were already demonstrated to be successful and scalable to form TS-1 microspheres with a hierarchical porosity (47). On the second hand, spray drying is also widely used to dry proteins for food and pharmaceutical applications (48–51). However, in the case of enzymes, spray drying often leads to denaturation, due to the relatively harsh conditions applied during drying (high temperature, liquid/air interfacial stress, shear stress) (52–55). Applying spray drying to process enzymes for biocatalysis as the targeted application is not straightforward because the fragile enzyme structure has to be maintained so that the catalytic activity is preserved.

To mitigate deactivation, enzyme stability has to be enhanced. Generally speaking, enzyme stability can be improved through immobilization on a support (56), through the formation of cross-linked enzyme aggregates (CLEAs) (57) or through the creation of enzyme mutants by directed evolution (58–61). Another technique that has recently gained interest to stabilize proteins is their complexation with polyelectrolytes (62). The formation of protein-polyelectrolyte complexes is a self-assembly process known for more than a decade (63,64) that is now used in drug formulation (65–67) or in layer-by-layer deposition methods (62). The spontaneous assembly of enzyme-polyelectrolyte complexes (EPCs) is directed by electrostatic and van der Waals forces (68,69). The polyelectrolyte, a positively- or negatively-charged polymer, coils around the enzyme which features a pH-dependent surface charge (70). This versatile technique can be used to control and stabilize the enzyme activity (63,71,72). For example, Maruyama et al. and Izaki et al. have both shown, respectively with protein-polyelectrolyte complexes and antibody-polyelectrolyte complexes, that the formation of these complexes leads to a better protein stabilization against thermally-induced denaturation and mechanical stress (73,74). Souza et al. also highlighted a decrease in the denaturation rate of complexed β-galactoxidase compared to the free enzyme when

exposed to low pH (75). These results prompted us to investigate the possible stabilization of GOx through the formation of EPCs, in the perspective of the preparation of a GOx/TS-1 hybrid catalyst by one-step spray drying.

In this work, a novel pathway is developed for the one-pot preparation of hybrid catalysts combining both an enzyme and a heterogeneous catalysis in one bifunctional solid (Scheme 1). More precisely, we aim to combine the GOx enzyme with TS-1 zeolite nanocrystals using spray drying as a rapid, scalable, and direct production method. To obtain an active chemo-biocatalyst, our strategy is to leverage on the stabilization effect of a polyelectrolyte, via the formation of EPCs. The obtained hybrid catalyst will be exploited for the *in situ* production of hydrogen peroxide and subsequent allyl alcohol epoxidation.

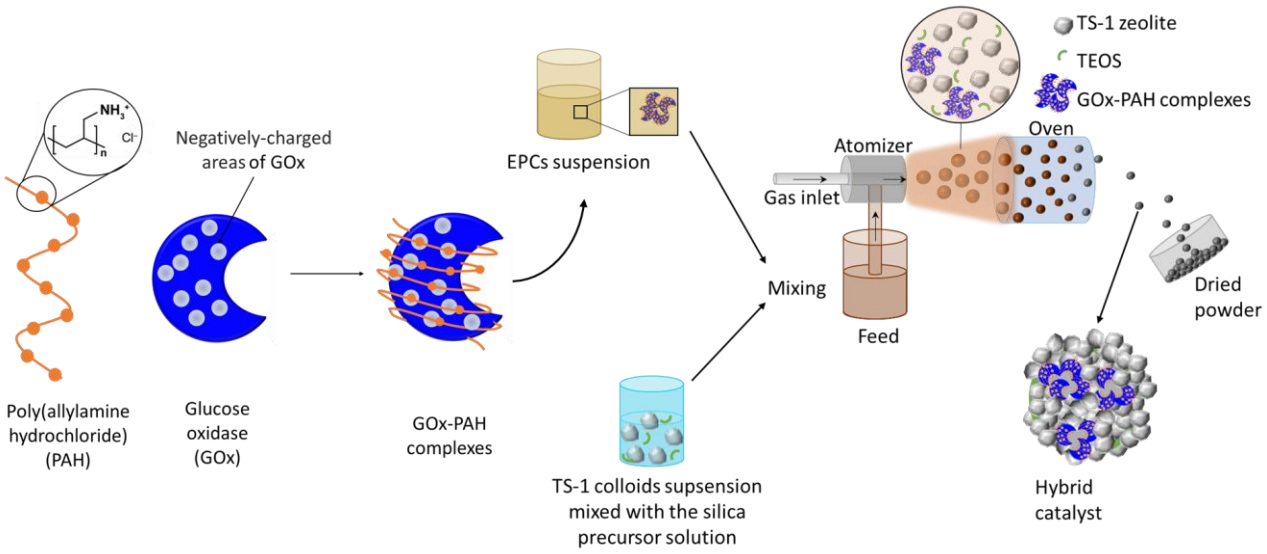

Scheme 1. Schematic representation of the one-pot synthesis strategy. The EPCs are primarily self-assembled by mixing the PAH and GOx. The TS-1 colloids suspension and the silica precursors solution, mixed beforehand, are mixed with the EPCs suspension and the hybrid catalyst is formed using the aerosol method.

Experimental

Materials

Titanium isopropoxide (TiiP; ≥ 98%), allyl alcohol (≥ 99%; extra pure), D-(+)-glucose (ACS reagent, anhydrous) and glycidol (≥ 96%) were purchased from Acros Organics. Tetraethyl orthosilicate (TEOS; ≥ 98%), Butan-1-ol (≥ 99.4%), hydrogen peroxide solution (H_2O_2; ≥ 30% w/w in H_2O), poly(allylamine hydrochloride) (PAH, average molar mass 17 500 $g.mol^{-1}$) and Bradford reagent were purchased from Sigma-Aldrich. Ethyl acetate (for gas chromatography ECD and FID) and tetrapropylammonium hydroxide (TPAOH; 40% in H_2O) were purchased from Merck. Titanium (IV) sulfate (≥ 15%) was purchased from Fisher Scientific. Hydrochloric acid (HCl; ≥ 37%) and isopropyl alcohol (PrOH) were respectively purchased from VWR Chemicals and VWR Life Sciences. Glucose oxidase (GOx) from *Aspergillus niger* was purchased from TCI. Distilled water was used for all synthesis and treatment processes.

TS-1 synthesis

The titanosilicalite-1 suspension was prepared via hydrothermal synthesis according to a protocol adapted from the literature (27,37,76). Solution A was prepared by solubilizing 0.55 g titanium isopropoxide in 5 g propyl alcohol. 22.5 g TEOS were mixed with 16.51 g aqueous solution of TPAOH (40% w/w) and 9.84 g distilled water to form solution B. Both solutions were stirred for 5 min before solution A was added dropwise to solution B. The turbid mixture was stirred for another 15 min before a solution composed of 5.47 g TPAOH and 38.25 g distilled H_2O was added. The resulting mixture was kept under stirring and heated at 75°C for 3h to evaporate the alcohol. Then, 30 mL distilled H_2O were added and the mixture was transferred into a 70 mL Teflon-lined stainless-steel autoclave for 24 h at 160°C. After rapid cooling, the resulting white precipitate was isolated by centrifugation and washed multiple times with distilled H_2O until

reaching neutral pH. The white solid was recovered and dried under vacuum overnight at 70°C and calcined under static air at 550°C for 5 h (heating rate of 5°C/min). The calcined powder was mixed with distilled water to obtain a 23% (w/w) colloidal suspension. TS-1 colloidal suspension was sonicated for 30 min and then kept under stirring at room temperature until use.

Formation of GOx-PAH complexes (EPCs suspension)

The enzyme-polyelectrolyte complexes (EPCs) were formed by mixing 3.8 mL of GOx solution (26.32 $mg.mL^{-1}$) and 2.66 mL of PAH solution (4.22 $mg.mL^{-1}$), brought to pH 6.5 with TPAOH (40%) beforehand, to reach a charge ratio (+)/(-) = 6.6 (details on the charge ratio calculations can be found in Figure S1).

Preparation of the hybrid catalysts in one pot by spray drying

A solution of silica precursor was synthesized by mixing 0.387 g TEOS, 5.993 g distilled water and 0.984 g HCl (0.012M). It was kept under vigorous stirring overnight to allow the pre-hydrolysis of the silicon alkoxide. Then, 4.36 g of TS-1 suspension (23% w/w) was added. This corresponds to a TS-1 : SiO_2 volume ratio of 9 : 1, where silica acts as the binder. The mixture was brought to pH 6.5 by addition of TPAOH (40%) and then stirred for 5 min. Then 3.309 g of the EPCs solution (corresponding to 50.1 mg of GOx) was added and the mixture was stirred for another 5 min. Then, the mixture was processed in a flow of air in a Büchi Mini Spray Dryer B-290 with an air pressure of 4 bars in a glass reactor heated at 50°C. This protocol was used to produce ~1.1 g hybrid catalyst in the form of a yellow powder which is denoted "**Hybrid_EPCs**" and has a nominal GOx loading of 45 $mg_{GOx}.g_{catalyst}^{-1}$. This hybrid is stored at 4°C.

The procedure was also applied, using a solution of free GOx (15.48 $mg.mL^{-1}$) instead of the EPCs solution, to obtain a hybrid catalyst called "**Hybrid_GOx**" with the same nominal loading

of 45 $mg_{GOx}.g_{catalyst}^{-1}$. Another control material was prepared by replacing the enzyme solution by water to obtain a reference inorganic catalyst called "**Aer_TS-1**".

Characterization

A Beckman Coulter DU800 Spectrophotometer was used to measure the turbidity of the suspension and thereby monitor the formation of EPCs. The effect of temperature and pH on their integrity was also investigated through spectrophotometry. 1 mL of GOx solution (26.32 $mg.mL^{-1}$) was put in a cuvette, increasing amounts of PAH solution (4.22 $mg.mL^{-1}$) were added and the absorbance was measured at 600 nm.

Nitrogen physisorption analyses were carried out at 77 K using a Tristar 3000 (Micromeritics, USA) instrument to determine de textural properties of the samples. Prior to analysis, the samples were degassed overnight under vacuum at 150°C. The specific surface area was determined by the BET method in the 0.05 – 0.30 p/p_0 range. The total pore volume is measured at $p/p_0 = 0.98$ and the micropores volume is determined via the t-plot. The pore size distribution is obtained from the adsorption part of the isotherm using the BJH method.

Scanning electron microscopy (SEM) analysis was performed using a JEOL 7600F microscope at 15.0 kV voltage. Samples were coated with a 15 nm layer of chromium with a Sputter Metal 208 HR (Cressington) under vacuum.

Dynamic Light Scattering (DLS) measurements were performed using a Malvern CGS-3 equipped with a He-Ne laser at a wavelength of 633nm and at a 90° scattering angle. The samples were analyzed as prepared (in water). Experiments were performed at room temperature and 10 readouts were taken and averaged for each sample.

Thermogravimetric analysis (TGA) was carried out on a TGA/DSC 3+ (Mettler Toledo) thermogravimetric apparatus. Samples were dried overnight at 120°C and measurements were

performed with the following program of analysis: purge under dry nitrogen for 2 min at 25°C, then dwell at 25°C in air for 10 min and finally, the temperature was increased from 25°C to 900°C (10°C.min^{-1}) in a dry air flow (100 mL.min^{-1}).

A modified Bradford assay was used to evaluate the amount of enzyme in solution. A calibration was performed by mixing 0.5 mL of Bradford reagent and 0.5 mL of GOx solution ranging from 0 to 0.1 mg.mL^{-1}. Absorbance was measured at 450 nm and 590 nm using a Thermo Scientific Genesys 10s Vis spectrophotometer and the value of A_{590nm}/A_{450nm} was plotted as a function of the enzyme amount (77,78). Leaching of the enzyme from the hybrid catalysts was evaluated using the same method. The hybrid catalysts were washed with distilled water and centrifuged to recover the supernatant and measure the enzyme concentration. Leaching tests were also performed on the filtered medium after the catalytic cascade test.

Biocatalytic production of H_2O_2, allyl alcohol epoxidation, and one-pot chemoenzymatic reaction

Enzymatic activity was measured based on the rate of oxygen consumption. O_2 concentration in the reactor was monitored using an OXY-4 fiber optic oxygen meter connected to an optical oxygen sensor PreSens GmbH fixed on the inner side of the vessel. Reaction medium was prepared in a 50 mL volumetric flask with 500 µl pH buffer (PBS, 1M) and glucose solution (200 mM) and the resulting reaction medium was transferred to a 100 mL glass reactor equipped with a magnetic stirrer. pH was adjusted to 6.0 with HCl (0.2 M) and the medium was saturated with O_2 by sparging oxygen (Air Liquide Alphagaz 1, purity 5.0) and kept at 45°C. The specific enzymatic activity is approximated by the initial O_2 consumption rate and normalized to the introduced amount of enzyme. The latter amount was chosen to determine the enzymatic activity taking into account the response time of the instrument. This test was performed at different pH and to evaluate the thermal

stability of the enzyme after different incubation times. In all the tests (either with free GOx, EPCs or with the hybrid catalysts), the enzyme loading was set to about 4.5 $mg.mL^{-1}$.

To evaluate the catalytic activity of the inorganic catalyst (TS-1), 9.152 g distilled H_2O, 0.528 g allyl alcohol (0.9 M), 0.037 g butan-1-ol (used as internal standard) and 50 mg of catalyst were mixed in a two-necked glass round-bottomed reactor heated at 45°C and equipped with a magnetic stirrer and a rubber septum. After 10 min, 180 µl aqueous H_2O_2 (30% w/w) were added with a syringe to initiate the reaction. Aliquots were collected at regular time intervals during the 3 h of analysis to monitor the formation of glycidol. Extraction was performed with ethyl acetate (10:90 v/v) to remove water and the samples were analyzed with a CP-3800 Gas Chromatography Varian Chrompack equipped with a FID detector and a capillary column (BR-5, 30 m, 0.32 mm i.d., 1.0 µm film thickness).

The cascade chemoenzymatic epoxidation of allyl alcohol was studied in a 100 mL glass reactor equipped with a thermostatic bath and a magnetic stirrer. The reaction medium was prepared with 5.28 g allyl alcohol, 0.373 g butan-1-ol and 81.46 glucose solution (200mM). The medium was saturated with oxygen by using a PDMS hollow fiber membrane fed with oxygen at 1 $l.h^{-1}$ rate. Once temperature was stabilized (45 °C), 11.9 mL of a suspension containing the hybrid catalyst (500 mg) was added. The pH of the reaction medium was maintained in the 5.5-6 range by addition of NaOH thanks to a TitroLine 7000 automatic titrator (Xylem Inc, Germany) to avoid acidification due to the production of gluconic acid. The reaction was monitored for 24 h by regular samplings. The amount of NaOH used for continuous titration was used to calculate the enzyme specific activity (production of gluconic acid). The conversion of allyl alcohol and the formation of glycidol was analyzed through gas chromatography. The production of H_2O_2 was measured by

colorimetric assay with 15% w/w titanium (IV) sulfate (Fischer Chemicals). The absorbance was measured at 405 nm using a Thermo Scientific Genesys 10s Vis Spectrophotometer.

Results and discussion

The results are presented and discussed in 3 distinct parts so that the two partners of the bifunctional hybrid catalyst are first described as separate entities, before being combined in the hybrid catalyst. Thus, the inorganic part of the catalyst is studied in the form of **TS-1** nanocrystals and TS-1 microspheres obtained by spray drying (thereafter called **Aer_TS-1**), and tested in the epoxidation of allyl alcohol. Then the enzyme is analyzed in its free (**GOx**) and complexed (**EPCs**) form, and tested in the oxidation of glucose. Finally, the two catalysts are combined to form the hybrid materials. Each step of the formation of the hybrid catalyst is discussed. The enzyme is incorporated either in its free or complexed form in the hybrid catalysts (**Hybrid_GOx** and **Hybrid_EPCs**), and these are tested in the cascade reaction.

*Study of the inorganic catalyst (**TS-1** and **Aer_TS-1**)*

As prepared titanium silicalite (**TS-1**) zeolites can be described as nanocrystals with dimensions between 100 and 150 nm (Figure S2 A), consistent with the size reported in the literature for such synthesis protocols (79,80). The microspheres obtained by the aggregation of these TS-1 nanocrystals via spray drying (**Aer_TS-1**) consist in spherical particles with a size ranging from 0.8 to 5 µm (Figure 1 A-B). Their shape results from the progressive drying of spherical aerosol droplets, leading to the formation spherical aggregates of TS-1 nanocrystals bound together by silica. Zooming in, the TS-1 nanocrystals are clearly visible (Figure S2 B). Their size is equal to

the size of the starting TS-1 nanocrystals (27). Interparticle voids are also observable between the aggregated nanocrystals with a size ranging from 40 to 65 nm.

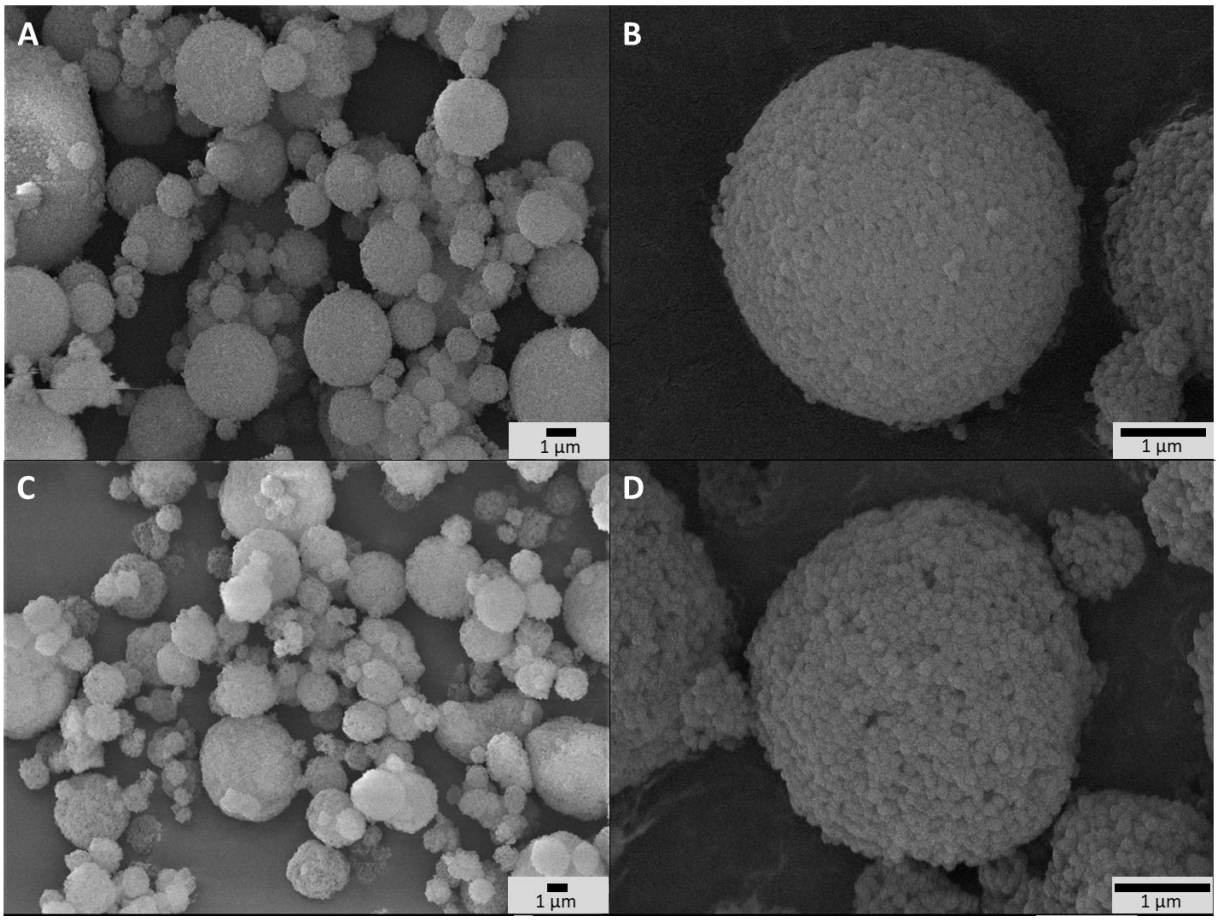

Figure 1. A-B) SEM images of **Aer_TS-1** at different magnifications. C-D) SEM images of **Hybrid_EPCs** at different magnifications.

N_2 adsorption-desorption isotherms of **TS-1** and **Aer_TS-1** are shown in Figure 2 along with the pore size distribution (PSD) computed from adsorption. For both samples, the strong N_2 uptake at low pressure accounts for the presence of micropores. While **TS-1** is microporous, as evidenced by the type I isotherm ($V_\mu = 0.14 \pm 0.01$ $cm^3.g^{-1}$), interparticular voids also contribute to the total volume ($V_p = 0.43 \pm 0.01$ $cm^3.g^{-1}$). According to the t-plot, the external specific surface area (i.e.

excluding the surface developed by micropores) is 126 ± 7 $m^2.g^{-1}$. Similarly, **Aer_TS-1** exhibits a micropore volume of 0.13 ± 0.01 $cm^3.g^{-1}$ showing that the microporous structure of the materials is preserved. However, the total pore volume is slightly reduced (0.30 ± 0.01 $cm^3.g^{-1}$), possibly accounting for the fact that the packing (and therefore the interparticles voids) is more compact when the TS-1 is processed in the spray drier, in the presence of the silica binder. The small hysteresis observed at high p/p_0 is representative of a type IV isotherm and is associated with the presence of a low amount of large mesopores in the 50-80 nm range created during the spray drying process (see insert in Figure 2). The external surface area is also decreased down to 82 ± 3 $m^2.g^{-1}$, possibly associated with the presence of the binder.

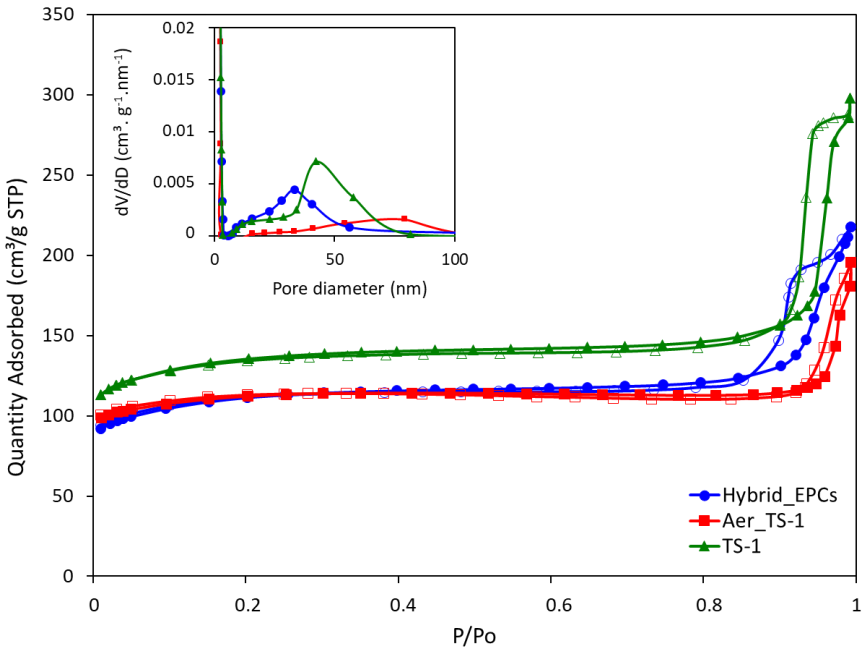

Figure 2. N_2 adsorption-desorption isotherms of TS-1, Aer_TS-1 and Hybrid_EPCs. In insert, the pore size distributions (PSDs) based on the BJH model are shown.

The catalytic activity of **TS-1** nanocrystals was evaluated in the reaction of allyl alcohol epoxidation with H_2O_2 as the oxidant. The final epoxide yield reached 73% after 180 min, and no trace of glycerol was found (Figure 3). This is consistent with the known excellent catalytic activity and selectivity of this zeolite for the epoxidation of light olefins in water (36,81,82). The level of activity is also in line with previously reported data (35,75).

When processed by spray drying, the obtained TS-1-based microspheres (here denoted **Aer_TS-1**) showed a slightly lower activity, with a final epoxide yield of 58% (Figure 3). However, it should be noted that this material also contains 10 vol.% of silica, used as a binder. Thus, normalizing the activity by the actual amount of TS-1 present in the sample, the epoxide production rate (calculated from the initial production of glycidol at 15 min) of **TS-1** and **Aer_TS-1** is respectively 26.6 and 25.0 mmol of glycidol per gram of TS-1 present in the material, showing that the intrinsic activity of the TS-1 nanocrystals is in fact maintained after spray drying. The selectivity toward glycidol is also fully preserved during the catalytic test. This result highlights that the active sites of each individual TS-1 crystals remains accessible in **Aer_TS-1** catalyst. It also indicates that the physico-chemical properties of TS-1 are not altered by the spray drying processing.

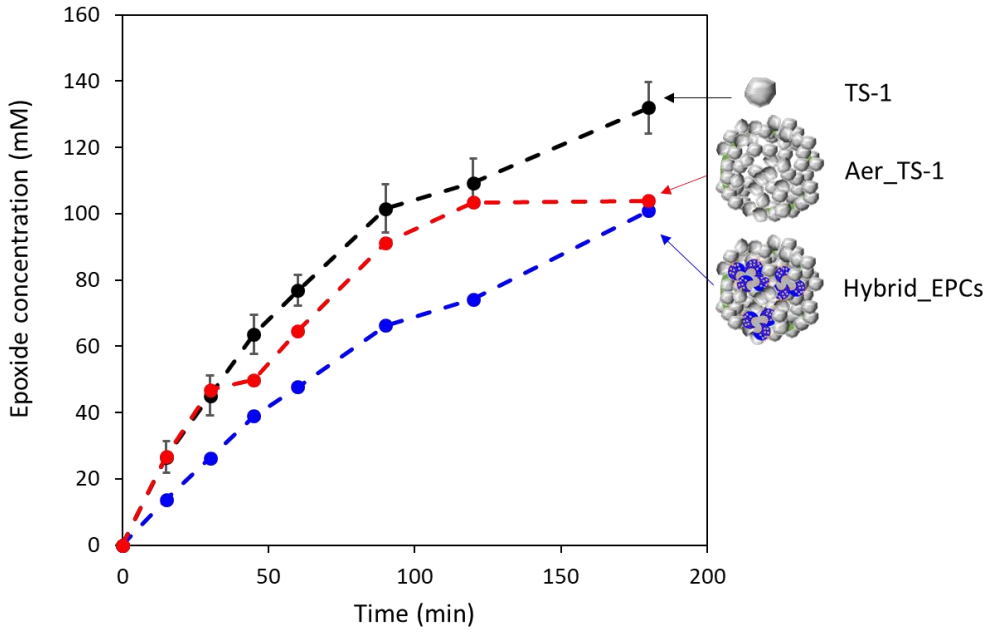

Figure 3. Kinetic data for the Ti-catalyzed conversion of allyl alcohol into glycidol in H_2O using aqueous solution of hydrogen peroxide as oxidant. Experimental conditions: T = 45°C, [cata] = 5 $g.L^{-1}$, [H_2O_2] = 0.18 M, [Allyl alcohol] = 0.9 M. The data obtained for TS-1 zeolite is the result of 3 catalytic tests independently performed. The experiment has been repeated three times with TS-1 to evaluate the experimental error on these measurements (see error bars).

*Study of the enzyme (**GOx** and **Enzyme-Polyelectrolyte Complexes (EPCs)**)*

The enzyme specific activity was measured at 45 °C and at its optimal pH (i.e. pH 6 (27)) through the consumption of oxygen during the reaction. **GOx** exhibited a specific activity of 146 $\mu mol_{O2}.min^{-1}.mg_{GOx}^{-1}$ (Figure 4).

In the perspective of spray drying, the complexation of GOx with poly(allylamine hydrochloride) (PAH) and its influence on the enzymatic activity was investigated. At pH 6, PAH is a positively-charged weak polyelectrolyte able to coil around the enzymes to make electrostatic interactions with the negative surface charges, thereby forming so-called enzyme-polyelectrolyte

complexes (EPCs) (64,70,83). Dynamic light scattering experiments were performed to measure the size of the EPCs and to determine the amount of polyelectrolyte that has to be added to the enzyme solution to ensure the complete complexation of GOx (i.e. no free GOx left in solution) (Figure S1). With 2.95 mg of PAH (corresponding to a charge ratio +/- of 6.6), no more signal of free GOx was detected, which means that all enzyme molecules were incorporated in the EPCs.

The specific enzymatic activity of the **EPCs** reached 95 $\mu mol_{O2}.min^{-1}.mg_{GOx}^{-1}$ (Figure 4), thus lower than for free **GOx**. This decrease is tentatively explained by the structure of the complexes where PAH is coiled around the enzyme molecules and may hinder the accessibility of the active sites. Also, the formation of **EPCs** can induce conformational change in the enzyme structure and some active sites might be impaired (84). Finally, the polyelectrolyte creates a microenvironment in which the local conditions (such as the pH) might be slightly different from the bulk of the solution and affect the enzymatic activity (80,85,86). Indeed, the degree of ionization of PAH can affect the local pH around and inside the EPCs (85). In the conditions chosen in this work, there is an excess of positive charges (charge ratio +/- = 6.6) so that the complexes are surrounded by positive charges that will affect the charge distribution in water. To support this claim, the enzymatic activity was also measured at pH 7 to compare the results of **GOx** and **EPCs** (Figure S3). Unlike **GOx** – which was much less active at pH 7 – the specific activity of **EPCs** remained almost identical at pH 6 and pH 7. Spectrophotometry measurements were performed to ensure that this effect was not induced by the release of GOx from the EPCs (Figure S4). These results tend to confirm that the formation of EPCs can affect the microenvironment around the enzymes and result in a certain stabilization of the latter.

The possible stabilization of GOx in the EPCs against thermally-induced deactivation was also investigated by measuring the enzymatic activity of free **GOx** and **EPCs** after different times (1-

5 h) of incubation at 45 °C (Figure S5). **EPCs** suffered from thermal deactivation similarly to free **GOx** after 5 h meaning that the formation of complexes did not protect the enzyme effectively against thermal denaturation.

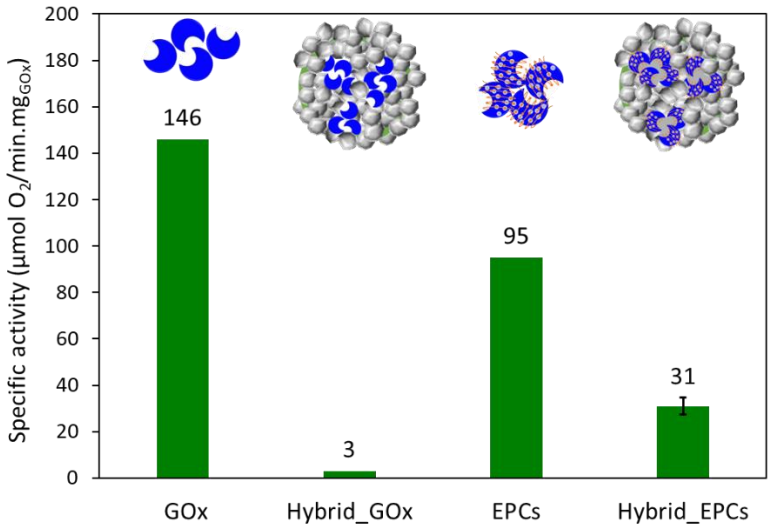

Figure 4. Comparison of the initial specific activity in GOx, EPCs and hybrid catalysts. Experimental conditions: T = 45°C, [Glucose] = 200mM, PBS buffer, pH 6. The experiment has been repeated three times with **Hybrid_EPCs** to evaluate the experimental error (see error bars, relative error = 11.6%).

*Study of hybrid catalysts (**Hybrid_GOx** and **Hybrid_EPCs**)*

First, a hybrid catalyst was synthesized in one-pot by the aerosol process with free GOx (**Hybrid_GOx**). The initial specific activity of GOx in **Hybrid_GOx** reached only 3 $\mu mol_{O2}.min^{-1}.mg_{GOx}^{-1}$ which corresponds to less than 2% of the initial specific activity of **GOx** (Figure 4). Thus, an almost complete enzyme deactivation occurred upon spray drying, even though the inlet gas was set at a low temperature (50°C) and the residence time in the drying chamber was short (~3 sec). As discussed in the literature (54), the important shear stress (as encountered in the nozzle of the spray drier) and the sudden transition from a liquid-solid interface to a gas-solid interface

(that occurs during drying) may be the cause of this deactivation. It should be noted that the enzyme was efficiently trapped into the hybrid materials, as a Bradford assay performed on the very pale yellow supernatant (Figure 5A) obtained after 3 washings of the hybrid catalyst showed that only 1.8% of GOx had leached from this sample (Figure 5 B). However, when the washed catalyst was re-tested, it showed no enzymatic activity at all, suggesting that the only enzyme molecules responsible for the low level of activity reported in Figure 4 were those that had leached out from the solid, subsequently acting as homogenous biocatalysts. In other words, even though GOx was effectively trapped in **Hybrid_GOx** through spray drying, it was totally deactivated, and such one-step preparation starting from the free enzyme is ineffective.

To alleviate the loss of enzymatic activity we investigated the possibility to protect the enzyme from the stress encountered during spray drying. Thus, a second type of hybrid catalyst (**Hybrid_EPCs**) was synthesized using GOx complexed with PAH (**EPCs**) instead of free GOx. The same spray drying conditions were applied. In SEM, this hybrid catalyst resembles **Aer_TS-1**: it consists in spherical aggregates of TS-1 with a size distribution ranging from 0.8 to 5 µm (Figure 1 C-D). TS-1 nanocrystals integrity is preserved in **Hybrid_EPCs** (Figure S2). This is further confirmed by N_2 physisorption analyses (Figure 2), since the micropore volume reached 0.12 $cm^3.g^{-1}$ and the external surface area was 125 $m^2.g^{-1}$, close to the value obtained for **TS-1**. Expectedly, the spray drying in the presence of the EPCs did not affect the textural properties of the TS-1 nanocrystals. The total pore volume is 0.33 $cm^3.g^{-1}$ which fits closely with the value obtained for **Aer_TS-1**. Pore size distribution (insert in Figure 2) shows smaller interparticle mesopores, in the 10 – 20 nm range, suggesting that the presence of the EPCs somewhat affects the way nanocrystals aggregate.

The specific enzymatic activity of **Hybrid_EPCs** reached 31 $\mu mol_{O2}.min^{-1}.mg_{GOx}^{-1}$, which has to be compared to the 95 $\mu mol_{O2}.min^{-1}.mg_{GOx}^{-1}$ reached by **EPCs** (Figure 4). This corresponds to a residual activity of 33%. In other words, while the unprotected GOx suffered a complete deactivation upon spray drying, about one third of the enzymatic activity of the EPCs was preserved. It can be said that the use of complexes effectively contributed to the stabilization of the enzyme against deactivation during spray drying. This finding is consistent with several reports from the literature that indicate a beneficial effect of complexation against deactivation (vs. thermal, mechanical, or chemical stress) (73,74). When measured at pH 7, the specific enzymatic activity of **Hybrid_EPCs** reached 29 $\mu mol_{O2}.min^{-1}.mg_{GOx}^{-1}$ which again confirms that EPCs are less sensitive to pH changes as compared to free GOx (Figure S3).

Hybrid_EPCs was subjected to a sequence of washing-centrifugation-Bradford assay and the amount of leached GOx in solution was measured in the supernatant. The latter supernatant was colorless (Figure 5A) and the total amount of leached GOx after 3 washings corresponded to about 0.1% of the total enzyme loading (Figure 5 B). On the contrary, the pellet obtained after centrifugation remained yellowish. This result shows that the interaction between GOx and PAH is strong enough to maintain the enzymes inside the hybrid material and avoid leaching. It represents another advantage of complexing GOx before spray drying. The experimental loading of EPCs in **Hybrid_EPCs** was evaluated by thermogravimetric analysis (Figure S6). The mass loss corresponding to the decomposition of GOx and PAH occurred between 200 and 750°C. The experimental loading obtained (53 $mg_{organic\ matter}.g_{catalyst}^{-1}$) roughly matched the theoretical one (50 $mg_{organic\ matter}.g_{catalyst}^{-1}$) showing that the spray drying process allows a precise control of the composition of the hybrid material.

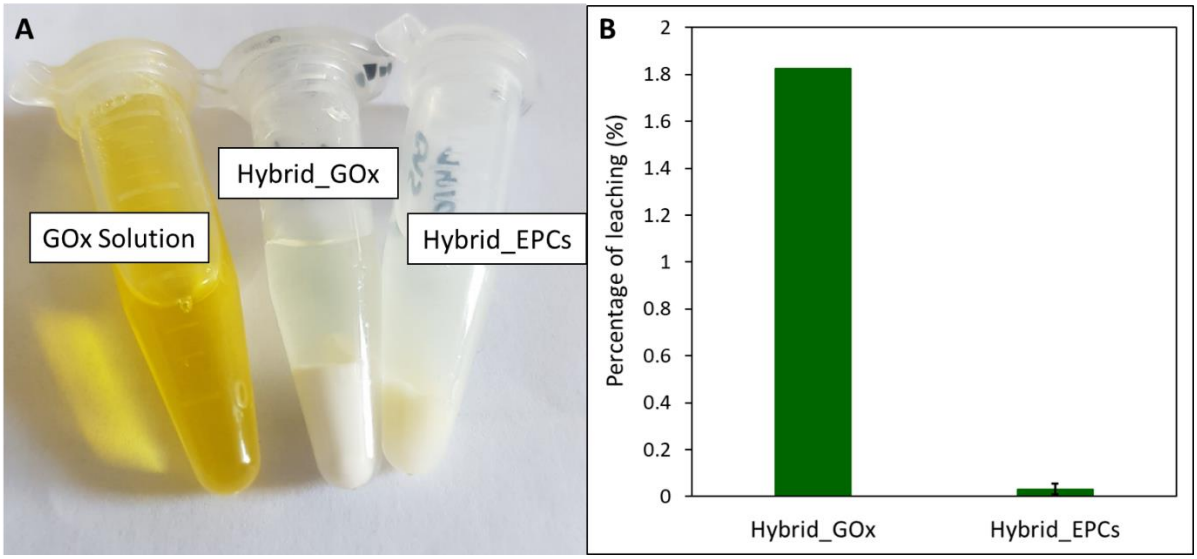

Figure 5. A)Pictures of the GOx solution (26.32 mg/ml), Hybrid_GOx and Hybrid_EPCs samples in suspension (100$mg_{catalyst}$/mL). **Hybrid_GOx** sample exhibits a very slighlty yellow supernatant and a clean white powder attributed to the leaching of GOx in solution. **Hybrid_EPCs** sample shows a clear supernatant with no apparent leaching and a slightly yellow powder proving that GOx is inserted in the hybrid material. B) Leaching of GOx from the hybrid material for **Hybrid_GOx** and **Hybrid_EPCs** after 24 h storage, measured by Bradford colorimetric assay.

The epoxidation activity of the TS-1 zeolite nanocrystals embedded in **Hybrid_EPCs** was measured to verify if the incorporation of EPCs affected the catalytic performance of the inorganic catalyst (Figure 3). The epoxide yield reached 56% after 180 minutes. Initial specific activity reached 12.8 $mmol.h^{-1}.g_{TS-1}^{-1}$ for **Hybrid_EPCs**, which has to be compared to 25.0 $mmol.h^{-1}.g_{TS-1}^{-1}$ for **Aer_TS-1**. This drop may be attributed to the fact that complexes integrated in the hybrid catalyst hinder the access to the active site of the zeolite nanocrystals.

To validate our approach, the hybrid catalyst was tested in the cascade reaction, i.e. the epoxidation of allyl alcohol carried out in the absence of externally-added hydrogen peroxide,

using the H_2O_2 produced *in situ* by the enzyme trapped in the hybrid catalyst (Figure 6A). In the conditions used for the cascade reaction, a purely inorganic catalyst is totally inactive (27). Here, the detection of glycidol proved that the chemoenzymatic epoxidation was indeed catalyzed by the hybrid catalyst. The production of glycidol reached the value of 48.9 mM after 24 h, corresponding to an epoxide yield of 30% whereas the glucose conversion was 50%. The selectivity for glycidol was estimated at 66% (the balance corresponds to the epoxide ring opening leading to glycerol). The experiment was repeated with a fresh **Hybrid_EPCs** sample and showed similar levels of activity (Figure S7A), indicating that the experimental error in this procedure accounts for approximately 10% in relative.

The catalytic performance reported here is higher than the one obtained by a two-pot synthesis using hollow zeolite microparticles and enzyme encapsulation in the form of CLEAs (glycidol yield of 37.4 mM) (27). Interestingly, the GOx in **Hybrid_EPCs** also showed a better resistance against deactivation during the cascade reaction. Indeed, the enzymes in **Hybrid_EPCs** were still active after 24 h of test, as attested by the continuous consumption of glucose. This contrasts with the rapid loss of enzymatic activity reported in the case of the hybrid catalyst based on CLEAs in hollow zeolite microspheres (27). In fact, GOx is known to suffer deactivation by the product (H_2O_2) (87). In the case of **Hybrid_EPCs**, however, the **EPCs** are intimately mixed with TS-1 nanocrystals, and we surmise that hydrogen peroxide is rapidly consumed by the epoxidation reaction thereby mitigating enzyme deactivation. Moreover, the EPCs structure might bring an additional protection against the accumulation of hydrogen peroxide around GOx.

A Bradford assay was performed on the filtered medium after the 24h test to estimate the leaching of GOx from **Hybrid_EPCs**. 3.5 $mg_{GOx}.g_{catalyst}^{-1}$ had leached during the catalytic test accounting for 8% of the initial GOx loading. This may tentatively be explained by a progressive

loss of the strong interactions that maintain GOx and PAH together in the complexes and in the hybrid material. Indeed, theses electrostatic interactions in EPCs can be strongly affected by a change in the ionic strength, which is increasing during the cascade test due to the production of gluconic acid and the concomitant addition of sodium hydroxide. It was actually already demonstrated that the addition of low molecular weight electrolytes, such as sodium, had a screening effect on the intermolecular interactions ensuring EPCs stability (88).

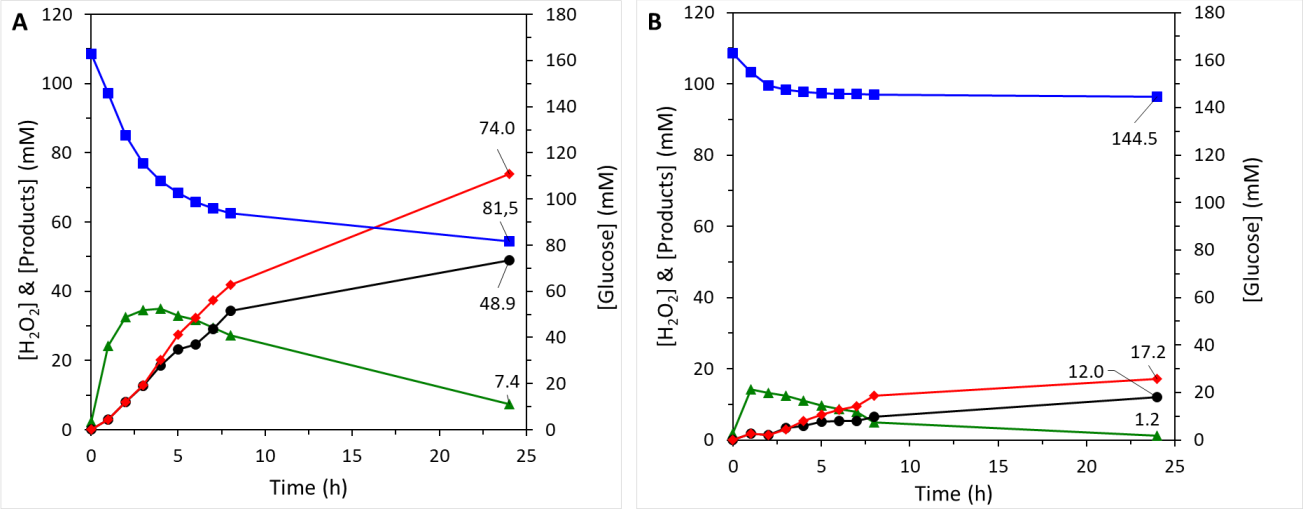

Figure 6. A) One-pot chemoenzymatic epoxidation of allyl alcohol with Hybrid_EPCs. Experimental conditions: T=45°C, [allyl alcohol] = 0.9 M, [Glucose] = 0.16 M, [Hybrid_EPCs] = 5.L^{-1}. B) One-pot chemoenzymatic epoxidation of allyl alcohol with the two separate catalytic species Aer_TS-1 and the PAH-GOx complexes. Experimental conditions: T=45°C, [allyl alcohol] = 0.9 M, [Glucose] = 0.16 M, [Aer_TS-1] = 5g.L^{-1}, [GOx-PAH complexes] = 0.048 g.L^{-1}. ▲ Hydrogen peroxide, ● glycidol, ■ Glucose, ♦ Total (Glycidol+Glycerol).

The same chemoenzymatic test was carried out with the two separate catalytic species composing the hybrid catalyst (*i.e.* **EPCs** and **Aer_TS-1**) (Figure 6B). The amount of each catalyst was adapted to reach the same conditions and thus the same intrinsic activity for each catalytic

species. The epoxide yield only reached 7% with a selectivity of 70%. The rapid stabilization of the glucose consumption rate indicates a fast deactivation of GOx in the **EPCs**. As mentioned, the formation of EPCs already brings protection to the enzymes, but the 24 h test at 45°C under the shear stress of recirculation via the pump might alter their structure, explaining the deactivation. In comparison, the encapsulation of EPCs in the TS-1 microspheres appears to bring a second protection against the different encountered stresses. These results highlight again that the preparation of a bifunctional material bearing two catalytic species is advantageous over the use of two separate catalysts.

Conclusions

In conclusion, we report a novel pathway for combining both an enzyme and a zeolite in one hybrid bifunctional material effective in a cascade chemoenzymatic reaction. We leverage on the spray drying process – as a rapid, direct, and continuous production method – to build TS-1 zeolites microspheres containing embedded glucose oxidase, in one step. The direct spray drying of the TS-1 suspension together with free GOx provokes the virtually complete deactivation of the enzyme. To obtain an active chemo-biocatalyst, we exploit the stabilization effect of a polyelectrolyte, via the formation of EPCs before spray drying. We report a strongly improved enzyme stability against the stress associated to spray drying, but also against leaching and against pH variations. The one-pot synthesized hybrid catalyst is active for the in situ production of hydrogen peroxide (by GOx) and the subsequent allyl alcohol epoxidation (by TS-1), reaching higher performance as compared to the systems already reported in the literature for this chemoenzymatic cascade reaction.

We anticipate that this strategy can be transposed to other catalytic systems and multistep cascade reactions. In fact, the integration of EPCs in hybrid materials is favored by the fact that,

while different enzymes may behave very differently upon assembly, the interactions of EPCs with other species are standardized in the reason of the presence of the polyelectrolyte shell that surrounds them. Thus, these results offer new perspectives, not only in the field of hybrid catalysts synthesis, but also in the broader field of multifunctional materials.

ASSOCIATED CONTENT
Supporting Information (PDF)

AUTHOR INFORMATION

Corresponding Author

Damien P. Debecker*

Institute of Condensed Matter and Nanosciences (IMCN), Université catholique de Louvain (UCLouvain) *e-mail : damien.debecker@uclouvain.be

Author Contributions

The manuscript was written through contributions of all authors. All authors have given approval to the final version of the manuscript.

Funding Sources

Any funds used to support the research of the manuscript should be placed here (per journal style).

Notes

Any additional relevant notes should be placed here.

ACKNOWLEDGMENT

M. Van der Verren is thankful to F.R.S.-FNRS for her PhD fellowship, under the project PDR–T.0058.19. V. Smeets and A. Vander Straeten are is thankful to F.R.S.–F.N.R.S. for their FRIA PhD grants. D.P. Debecker thanks the Francqui foundation for the "Francqui Research Professor" chair. Prof. Patrick Gerin is gratefully acknowledged for providing access to the optical oxygen sensor. F. Devred is acknowledged for the technical and logistical support.

REFERENCES

1. Beach ES, Cui Z, Anastas PT. Green Chemistry: A design framework for sustainability. Energy & Environmental Science. 2009; 2(10): 1038.

2. Centi G, Perathoner S. Catalysis and sustainable (green) chemistry. Catalysis Today. 2003; 77(4): 287–97.

3. Anastas P, Eghbali N. Green Chemistry: Principles and Practice. Chem Soc Rev. 2010; 39(1): 301–12.

4. Gérardy R, Debecker DP, Estager J, Luis P, Monbaliu J-CM. Continuous Flow Upgrading of Selected C_2 –C_6 Platform Chemicals Derived from Biomass. Chemical Reviews. 2020; In press, DOI: 10.1021/acs.chemrev.9b00846.

5. Rudroff F, Mihovilovic MD, Gröger H, Snajdrova R, Iding H, Bornscheuer UT. Opportunities and challenges for combining chemo- and biocatalysis. Nat Catal. 2018; 1(1): 12–22.

6. Turner NJ. Directed evolution of enzymes for applied biocatalysis. Trends in Biotechnology. 2003; 21(11): 474–8.

7. Singh R, Kumar M, Mittal A, Mehta PK. Microbial enzymes: industrial progress in 21st century. 3 Biotech. 2016; 6(2).

8. Singhania RR, Patel AK, Thomas L, Goswami M, Giri BS, Pandey A. Industrial Enzymes. In: Industrial Biorefineries & White Biotechnology. Elsevier; 2015. p. 473–97.

9. Andualema B, Gessesse A. Microbial Lipases and Their Industrial Applications: Review. Biotechnology(Faisalabad). 2012; 11(3): 100–18.

10. Thapa S, Li H, OHair J, Bhatti S, Chen F-C, Nasr KA, et al. Biochemical Characteristics of Microbial Enzymes and Their Significance from Industrial Perspectives. Molecular Biotechnology. 2019; 61(8): 579–601.

11. Gurung N, Ray S, Bose S, Rai V. A Broader View: Microbial Enzymes and Their Relevance in Industries, Medicine, and Beyond. BioMed Research International. 2013; 1–18.

12. Raveendran S, Ummalyma SB, Mathew AK, Madhavan A, Rebello S, Pandey A. Applications of Microbial Enzymes in Food Industry. Food Technology and Biotechnology. 2018; 56(1).

13. Sheldon RA, Brady D. Broadening the Scope of Biocatalysis in Sustainable Organic Synthesis. ChemSusChem. 2019; 12(13): 2859–81.

14. Sheldon RA, Brady D. The limits to biocatalysis: pushing the envelope. Chemical Communications. 2018; 54(48): 6088–104.

15. Zhang W, Fernández-Fueyo E, Ni Y, van Schie M, Gacs J, Renirie R, et al. Selective aerobic oxidation reactions using a combination of photocatalytic water oxidation and enzymatic oxyfunctionalizations. Nature Catalysis. 2018; 1(1): 55–62.

16. Freakley SJ, Kochius S, van Marwijk J, Fenner C, Lewis RJ, Baldenius K, et al. A chemo-enzymatic oxidation cascade to activate C–H bonds with in situ generated H2O2. Nature Communications. 2019; 10(1).

17. Huang H, Denard CA, Alamillo R, Crisci AJ, Miao Y, Dumesic JA, et al. Tandem Catalytic Conversion of Glucose to 5-Hydroxymethylfurfural with an Immobilized Enzyme and a Solid Acid. ACS Catalysis. 2014; 4(7): 2165–8.

18. Li X, Cao Y, Luo K, Sun Y, Xiong J, Wang L, et al. Highly active enzyme–metal nanohybrids synthesized in protein–polymer conjugates. Nature Catalysis. 2019; 2(8): 718–25.

19. Li X, Cao X, Xiong J, Ge J. Enzyme–Metal Hybrid Catalysts for Chemoenzymatic Reactions. Small. 2019; 1902751.

20. Gimbernat A, Guehl M, Capron M, Lopes Ferreira N, Froidevaux R, Girardon J-S, et al. Hybrid Catalysis: A Suitable Concept for the Valorization of Biosourced Saccharides to Value-Added Chemicals. ChemCatChem. 2017; 9(12): 2080–4.

21. Dumeignil F, Guehi M, Gimbernat A, Capron M, Lopes Ferreira N, Froidevaux R, et al. From sequential chemoenzymatic synthesis to integrated hybrid catalysis : taking the best of both worlds to open up the scope of possibilities for a sustainable future. Catalysis Science & Technology. 2018; 1–27.

22. Ye R, Zhao J, Wickemeyer BB, Toste FD, Somorjai GA. Foundations and strategies of the construction of hybrid catalysts for optimized performances. Nature Catalysis. 2018; 1(5): 318–25.

23. Wang Y, Ren H, Zhao H. Expanding the boundary of biocatalysis: design and optimization of *in vitro* tandem catalytic reactions for biochemical production. Critical Reviews in Biochemistry and Molecular Biology. 2018; 53(2): 115–29.

24. Sperl JM, Carsten JM, Guterl J-K, Lommes P, Sieber V. Reaction Design for the Compartmented Combination of Heterogeneous and Enzyme Catalysis. ACS Catalysis. 2016; 6(10): 6329–34.

25. Balistreri N, Gaboriau D, Jolivalt C, Launay F. Covalent immobilization of glucose oxidase on mesocellular silica foams: Characterization and stability towards temperature and organic solvents. Journal of Molecular Catalysis B: Enzymatic. 2016; 127: 26–33.

26. Vennestrøm PNR, Taarning E, Christensen CH, Pedersen S, Grunwaldt J-D, Woodley JM. Chemoenzymatic Combination of Glucose Oxidase with Titanium Silicalite-1. ChemCatChem. 2010; 2: 943–5.

27. Smeets V, Baaziz W, Ersen O, Gaigneaux EM, Boissière C, Sanchez C, et al. Hollow zeolite microspheres as a nest for enzymes: a new route to hybrid heterogeneous catalysts. Chemical Science. 2020; 11(4): 954–961.

28. Engström K, Johnston EV, Verho O, Gustafson KPJ, Shakeri M, Tai C-W, et al. Co-immobilization of an Enzyme and a Metal into the Compartments of Mesoporous Silica for Cooperative Tandem Catalysis: An Artificial Metalloenzyme. Angewandte Chemie International Edition. 2013; 52(52): 14006–10.

29. Zhang X, Jing L, Chang F, Chen S, Yang H, Yang Q. Positional immobilization of Pd nanoparticles and enzymes in hierarchical yolk–shell@shell nanoreactors for tandem catalysis. Chemical Communications. 2017; 53(55): 7780–3.

30. Ennaert T, Van Aelst J, Dijkmans J, De Clercq R, Schutyser W, Dusselier M, et al. Potential and challenges of zeolite chemistry in the catalytic conversion of biomass. Chemical Society Reviews. 2016; 45(3): 584–611.

31. Přech J. Catalytic performance of advanced titanosilicate selective oxidation catalysts – a review. Catalysis Reviews. 2018; 60(1): 71–131.

32. Wang J-J, Chuang Y-Y, Hsu H-Y, Tsai T-C. Toward industrial catalysis of zeolite for linear alkylbenzene synthesis: A mini review. Catalysis Today. 2017; 298: 109–16.

33. Vennestrøm PNR, Christensen CH, Pedersen S, Grunwaldt J-D, Woodley JM. Next-Generation Catalysis for Renewables: Combining Enzymatic with Inorganic Heterogeneous Catalysis for Bulk Chemical Production. ChemCatChem. 2010; 2(3): 249–58.

34. Vayssilov GN. Structural and Physicochemical Features of Titanium Silicalites. Catalysis Reviews. 1997; 39(3): 209–51.

35. Drago RS, Dias SC, McGilvray JM, Mateus ALML. Acidity and Hydrophobicity of TS-1. The Journal of Physical Chemistry B. 1998; 102(9): 1508–14.

36. Clerici MG, Ingallina P. Epoxidation of Lower Olefins with Hydrogen Peroxide and Titanium Silicalite. Journal of Catalysis. 1993; 140(1): 71–83.

37. Smeets V, Gaigneaux EM, Debecker DP. Hierarchical micro-/macroporous TS-1 zeolite epoxidation catalyst prepared by steam assisted crystallization. Microporous and Mesoporous Materials. 2020; 293: 109801.

38. Debecker DP, Le Bras S, Boissière C, Chaumonnot A, Sanchez C. Aerosol processing: a wind of innovation in the field of advanced heterogeneous catalysts. Chem Soc Rev. 2018; 47(11): 4112–4155.

39. Godard N, Vivian A, Fusaro L, Cannavicci L, Aprile C, Debecker DP. High-Yield Synthesis of Ethyl Lactate with Mesoporous Tin Silicate Catalysts Prepared by an Aerosol-Assisted Sol–Gel Process. ChemCatChem. 2017; 9(12): 2211–2218.

40. Aghamohammadi S, Haghighi M. Spray-dried zeotype/clay nanocatalyst for methanol to light olefins in fluidized bed reactor: Comparison of active and non-active filler. Applied Clay Science. 2019; 170: 70–85.

41. Kim A, Sanchez C, Haye B, Boissière C, Sassoye C, Debecker DP. Mesoporous TiO2 Support Materials for Ru-Based CO2 Methanation Catalysts. ACS Appl Nano Mater. 2019; 2(5): 3220–3230.

42. Li R, Yang Y, Sun N, Kuai L. Mesoporous Cu-Ce-O $_x$ Solid Solutions from Spray Pyrolysis for Superior Low-Temperature CO Oxidation. Chemistry – A European Journal. 2019; 25(68): 15586–93.

43. Ramesh S, Debecker DP. Room temperature synthesis of glycerol carbonate catalyzed by spray dried sodium aluminate microspheres. Catalysis Communications. 2017; 97: 102–105.

44. Smeets V, Boissière C, Sanchez C, Gaigneaux EM, Peeters E, Sels BF, et al. Aerosol Route to TiO2–SiO2 Catalysts with Tailored Pore Architecture and High Epoxidation Activity. Chem Mater. 2019; 31(5): 1610–1619.

45. Zelcer A, Franceschini EA, Lombardo MV, Lanterna AE, Soler-Illia GJAA. A general method to produce mesoporous oxide spherical particles through an aerosol method from aqueous solutions. Journal of Sol-Gel Science and Technology. 2019

46. Maksasithorn S, Praserthdam P, Suriye K, Debecker DP. Preparation of super-microporous WO3–SiO2 olefin metathesis catalysts by the aerosol-assisted sol–gel process. Microporous and Mesoporous Materials. 2015; 213: 125–133.

47. Niu C, Liu M, Gao X, Ye X, Wen Y, Liu Y, et al. Fabrication of Microspheres by Nano-TS-1 Crystals via a Spray-Forming Process: From Screening to Scale-up. ACS Omega. 2019; 4(2): 4397–4404.

48. Sosnik A, Seremeta KP. Advantages and challenges of the spray-drying technology for the production of pure drug particles and drug-loaded polymeric carriers. Advances in Colloid and Interface Science. 2015; 223: 40–54.

49. Arpagaus C, Collenberg A, Ruetti D, Assadpour E, Mahdi Jafari S. Nano Spray Drying for Encapsulation of Pharmaceuticals. International Journal of Pharmaceutics. 2018; 546.

50. Yoshii H, Buche F, Takeuchi N, Terrol C, Ohgawara M, Furuta T. Effects of protein on retention of ADH enzyme activity encapsulated in trehalose matrices by spray drying. Journal of Food Engineering. 2008; 87(1): 34–39.

51. Mohtar NS, Abdul Rahman MB, Mustafa S, Mohamad Ali MS, Raja Abd. Rahman RNZ. Spray-dried immobilized lipase from *Geobacillus* sp. strain ARM in sago. PeerJ. 2019; 7: e6880.

52. Lauruengtana V, Paramita V, Neoh TL, Furuta T, Yoshii H. Encapsulation of Enzymes by Spray Drying. Japan Journal of Food Engineering. 2009; 10(2): 79–85.

53. Chinnaswamy A, Rielly C, Stapley A. Effects of Process Variables on the Denaturation of Whey Proteins during Spray Drying. Drying Technology. 2007; 25: 799–807.

54. Maa Y-F, C. Hsu C. Protein Denaturation by Combined Effect of Shear and Air-Liquid Interface. Biotechnology and bioengineering. 1997; 54: 503–512.

55. Samborska K, Witrowa-Rajchert D, Gonçalves A. Spray-Drying of α-Amylase - The Effect of Process Variables on the Enzyme Inactivation. Drying Technology. 2005; 23(4): 941–953.

56. Mohamad NR, Marzuki NHC, Buang NA, Huyop F, Wahab RA. An overview of technologies for immobilization of enzymes and surface analysis techniques for immobilized enzymes. Biotechnology & Biotechnological Equipment. 2015; 29(2): 205–220.

57. Sheldon RA, Schoevaart R, Van Langen LM. Cross-linked enzyme aggregates (CLEAs): A novel and versatile method for enzyme immobilization (a review). Biocatalysis and Biotransformation. 2005; 23(3–4): 141–147.

58. Homaei AA, Sariri R, Vianello F, Stevanato R. Enzyme immobilization: an update. Journal of Chemical Biology. 2013; 6(4): 185–205.

59. Nisha S, Karthick A, Nallathambi G. A Review on Methods, Application and Properties of Immobilized Enzyme. Chemical Science Review and Letters. 2012; (1): 148-155.

60. Reetz MT. What are the Limitations of Enzymes in Synthetic Organic Chemistry? The Chemical Record. 2016; 16(6): 2449–59.

61. Porter JL, Rusli RA, Ollis DL. Directed Evolution of Enzymes for Industrial Biocatalysis. ChemBioChem. 2016; 17(3): 197–203.

62. vander Straeten A, Bratek-Skicki A, Germain L, D'Haese C, Eloy P, Fustin C-A, et al. Protein–polyelectrolyte complexes to improve the biological activity of proteins in layer-by-layer assemblies. Nanoscale. 2017; 9(44): 17186–17192.

63. Xia J, Dubin PL. Protein-Polyelectrolyte Complexes. In: Dubin P, Bock J, Davis R, Schulz DN, Thies C, editors. Macromolecular Complexes in Chemistry and Biology [Internet]. Berlin, Heidelberg: Springer Berlin Heidelberg; 1994. p. 247–71.

64. Cooper CL, Dubin PL, Kayitmazer AB, Turksen S. Polyelectrolyte–protein complexes. Current Opinion in Colloid & Interface Science. 2005; 10(1–2): 52–78.

65. Wan X, Liu T, Hu J, Liu S. Photo-Degradable, Protein-Polyelectrolyte Complex-Coated, Mesoporous Silica Nanoparticles for Controlled Co-Release of Protein and Model Drugs. Macromolecular Rapid Communications. 2013; 34(4): 341–347.

66. Kurinomaru T, Shiraki K. Aggregative protein–polyelectrolyte complex for high-concentration formulation of protein drugs. International Journal of Biological Macromolecules. 2017; 100: 11–7.

67. Shiraki K, Kurinomaru T, Tomita S. Wrap-and-Strip Technology of Protein–Polyelectrolyte Complex for Biomedical Application. Current Medicinal Chemistry. 2016; 23(3): 276–89.

68. Nita LE, Chiriac AP, Stoleru E, Diaconu A, Tudorachi N. Tailorable polyelectrolyte protein complex based on poly(aspartic acid) and bovine serum albumin. Designed Monomers and Polymers. 2016; 19(7): 596–606.

69. Caruso F, Schüler C. Enzyme Multilayers on Colloid Particles: Assembly, Stability, and Enzymatic Activity. Langmuir. 2000; 16(24): 9595–9603.

70. Choi J, Rubner MF. Influence of the Degree of Ionization on Weak Polyelectrolyte Multilayer Assembly. Macromolecules. 2005; 38(1): 116–24.

71. Larionova NI, Unksova LY, Mironov VA, Sakharov IY, Kazanskaya NF, Berezin IV. Investigation of complex formation between soluble carboxymethyl ethers of polysaccharides and proteins. Polymer Science USSR. 1981; 23(8): 1999–2006.

72. vander Straeten A, Bratek-Skicki A, Jonas AM, Fustin C-A, Dupont-Gillain C. Integrating Proteins in Layer-by-Layer Assemblies Independently of their Electrical Charge. ACS Nano. 2018; 12(8): 8372–81.

73. Maruyama T, Izaki S, Kurinomaru T, Handa K, Kimoto T, Shiraki K. Protein-poly(amino acid) precipitation stabilizes a therapeutic protein l-asparaginase against physicochemical stress. Journal of Bioscience and Bioengineering. 2015; 120(6): 720–724.

74. Izaki S, Kurinomaru T, Handa K, Kimoto T, Shiraki K. Stress Tolerance of Antibody–Poly(Amino Acid) Complexes for Improving the Stability of High Concentration Antibody Formulations. Journal of Pharmaceutical Sciences. 2015; 104(8): 2457–2463.

75. Souza CJF, Garcia-Rojas EE, Favaro-Trindade CS. Lactase (β-galactosidase) immobilization by complex formation: Impact of biopolymers on enzyme activity. Food Hydrocolloids. 2018; 83: 88–96.

76. Thangaraj A, Eapen MJ, Sivasanker S, Ratnasamy P. Studies on the synthesis of titanium silicalite, TS-1. Zeolites. 1992; 12(8): 943–950.

77. Zor T, Selinger Z. Linearization of the Bradford Protein Assay Increases Its Sensitivity: Theoretical and Experimental Studies. Analytical Biochemistry. 1996; 236(2): 302–308.

78. Bradford M. A Rapid and Sensitive Method for the Quantitation of Microgram Quantities of Protein Utilizing the Principle of Protein-Dye Binding. Analytical Biochemistry. 1976; 72(1–2): 248–54.

79. Xue Y, Wen Y, Huijuan W, Liu M, Huang X, Ye X, et al. Hollow TS-1 mesocrystals: hydrothermal construction and high catalytic performances in cyclohexanone ammoximation. RSC Adv. 2015; 5.

80. Zhang G, Sterte J, Schoeman BJ. Preparation of Colloidal Suspensions of Discrete TS-1 Crystals. Chemistry of Materials. 1997; 9(1): 210–217.

81. Murugavel R, Roesky HW. Titanosilicates: Recent Developments in Synthesis and Use as Oxidation Catalysts. Angewandte Chemie International Edition. 1997; 36(5): 477–9.

82. Clerici MG. The activity of titanium silicalite-1 (TS-1): Some considerations on its origin. Kinetics and Catalysis. 2015; 56(4): 450–455.

83. Kayitmazer AB, Seeman D, Minsky BB, Dubin PL, Xu Y. Protein–polyelectrolyte interactions. Soft Matter. 2013; 9(9): 2553.

84. Cousin F, Gummel J, Ung D, Boué F. Polyelectrolyte−Protein Complexes: Structure and Conformation of Each Specie Revealed by SANS. Langmuir. 2005; 21(21): 9675–88.

85. Zhang Y, Wang Q, Hess H. Increasing Enzyme Cascade Throughput by pH-Engineering the Microenvironment of Individual Enzymes. ACS Catalysis. 2017; 7(3): 2047–2051.

86. Goldstein L, Levin Y, Katchalski E. A Water-insoluble Polyanionic Derivative of Trypsin. II. Effect of the Polyelectrolyte Carrier on the Kinetic Behavior of the Bound Trypsin. Biochemistry. 1964; 3(12): 1913–1919.

87. Kleppe K. The Effect of Hydrogen Peroxide on Glucose Oxidase from Aspergillus niger. Biochemistry. 1966; 5(1): 139–43.

88. de Vasconcelos CL, Bezerril PM, dos Santos DES, Dantas TNC, Pereira MR, Fonseca JLC. Effect of Molecular Weight and Ionic Strength on the Formation of Polyelectrolyte Complexes Based on Poly(methacrylic acid) and Chitosan. Biomacromolecules. 2006; 7(4): 1245–1252.

Supporting Information

Hybrid chemo-biocatalysts prepared in one step from zeolite nanocrystals and enzyme-polyelectrolyte complexes

*Margot Van der Verren, Valentin Smeets, Aurélien vander Straeten, Christine C. Dupont-Gillain, Damien P. Debecker**

Institute of Condensed Matter and Nanosciences (IMCN), Université catholique de Louvain (UCLouvain) *e-mail : damien.debecker@uclouvain.be

Study and calculations of the charge ratio in the EPCs

Formation of the EPCs

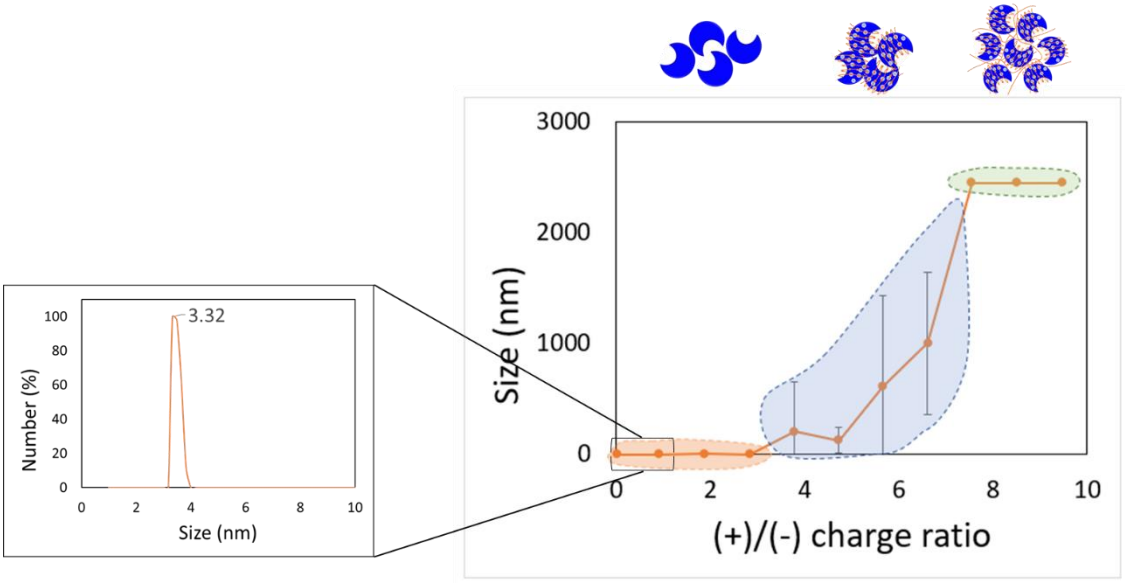

Figure S1. Measurements of the different size of the GOx-PAH complexes depending on the charge ratio. The measurements were performed by dynamic light scattering, on a solution of GOx (26.32 mg/ml) with increasing amount of a solution of PAH (4.22 mg/ml) and each measurement was repeated 10 times. The curve can be divided into 3 regions. In the first region (orange), GOx is mainly free in the solution and very small complexes are formed. The second region (blue) is a transition region where the size of the complexes is increasing with the charge ratio and thus the amount of PAH added. In the last region (green), the complexes are big enough to precipitate. The selected ratio is (+)/(-)=6.6 as it appears that no more free GOx was detected in solution.

Charge ratio calculations

The charge ratio is calculated as followed:

PAH charge calculations

Molar mass = 17 500 g.mol^{-1}

Based on the structure of PAH, the molar mass of one monomer unit can be calculated (=93.5 $g.mol^{-1}$) and the number of units in one molecule of PAH is calculated as follow:

$$N = \frac{Total\ M_w}{M_w of\ one\ unit} = 187.16\ units \quad (1)$$

Each unit carries a positive charge from the NH_3^+ group and therefore, each molecule of PAH bear **187.16** positive charges. The number of positive charges/mol is obtained by:

$$\left[\frac{(+)charges}{mol}\right] = 187.16 \frac{(+)charges}{molecule} * N_A = 1.12 * 10^{26} \quad (2)$$

GOx calculations

Molecular weight = 160 000 Da

The number of charges carried by each GOx molecule depends on the pH. These values are found on PDB2PQR (Code: 1CF3, GLUCOSE OXIDASE FROM APERGILLUS NIGER). At pH 6.0, each subunit carries 14.52 negative charges. The number of negative charges/mol is calculated following Equation 2.

(+)/(-) charge ratio

Depending on the concentration of each solution (PAH and GOx), the numbers of positive and negatives charges are calculated.

Study of the inorganic catalyst (TS-1 and Aer_TS-1)

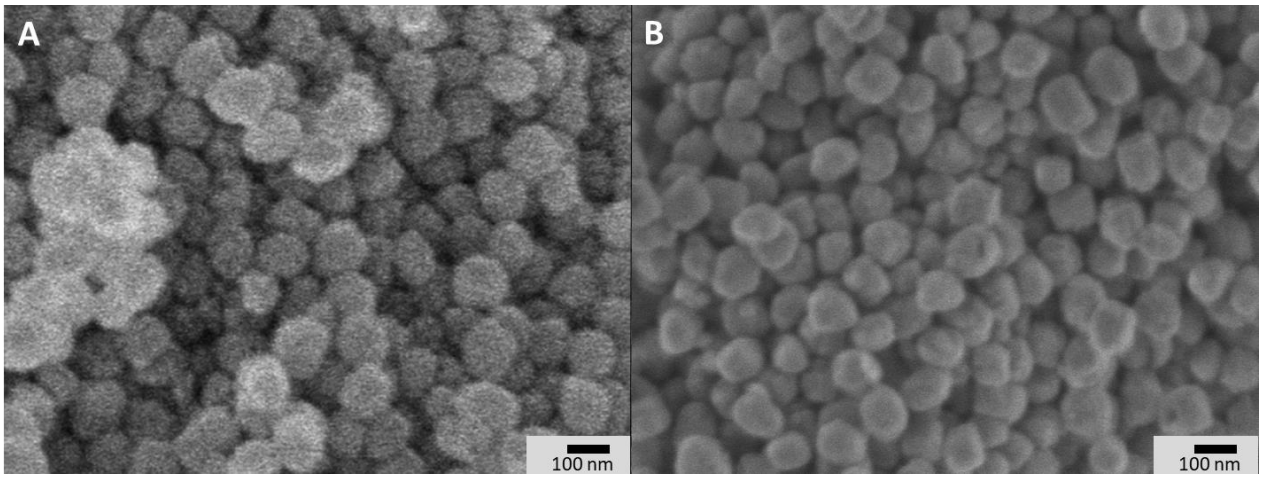

Figure S2. A) SEM images of TS-1 nanocrystals. B) SEM images of Hybrid_EPCs. Experimental conditions: powders were metallized with chrome. Image A) was measured at 5.0 kV and image B) was measured at 1.0 kV

Study of the organic catalyst in its different forms (GOx, EPCs, Hybrid_GOx and Hybrid_EPCs)

Stability toward pH and thermal variations

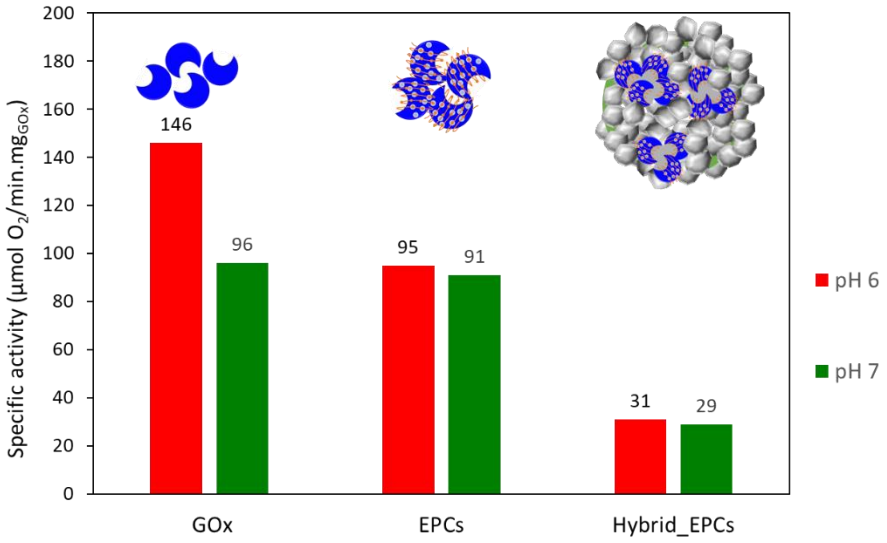

Figure S3. Comparison of the specific activity of the samples **GOx**, **EPCs**, and **Hybrid_EPCs** at pH 6 and pH 7. This figure highlights the stabilization effect toward pH variation brought by the formation of EPCs. Experimental conditions: T = 45°C, [Glucose] = 200mM

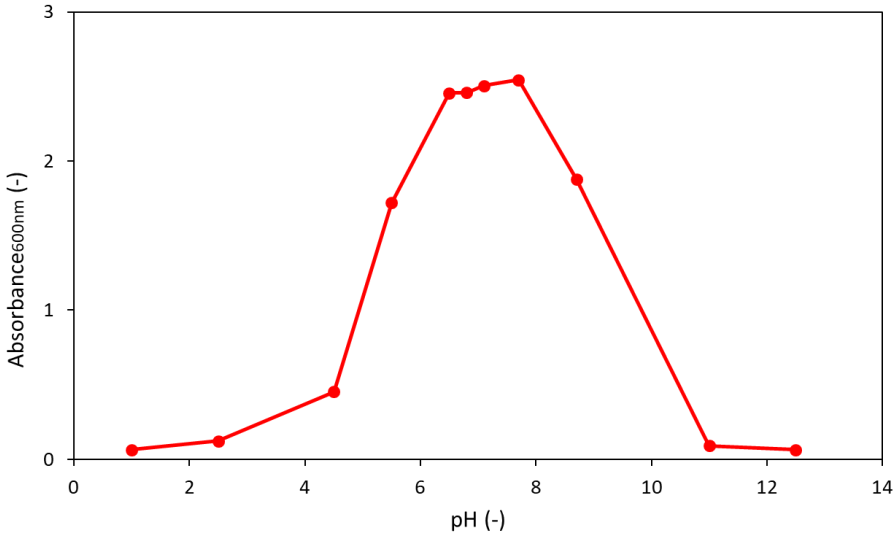

Figure S4. Study of the pH range in which the **EPCs** are stable. The absorbance of an EPCs suspension was measured at 600 nm at different pH. It shows that the EPCs are stable in a pH range between 5.8 and 8.

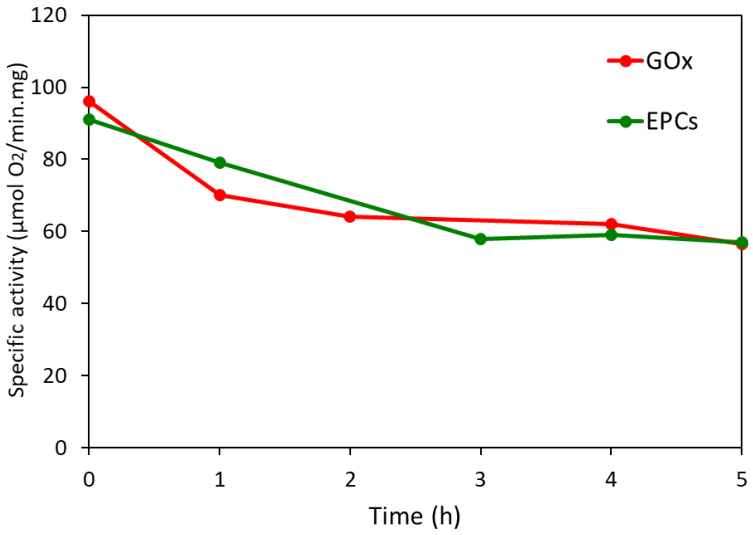

Figure S5. Stability of **GOx** and **EPCs** toward thermal denaturation. Experimental conditions: A solution of GOx and a suspension of EPCs (15.48 $mg_{GOx}.mL^{-1}$) were placed in a 45°C hot bath. The enzymatic activity was tested at regular interval of time to see the influence of thermal denaturation.

GOx loading

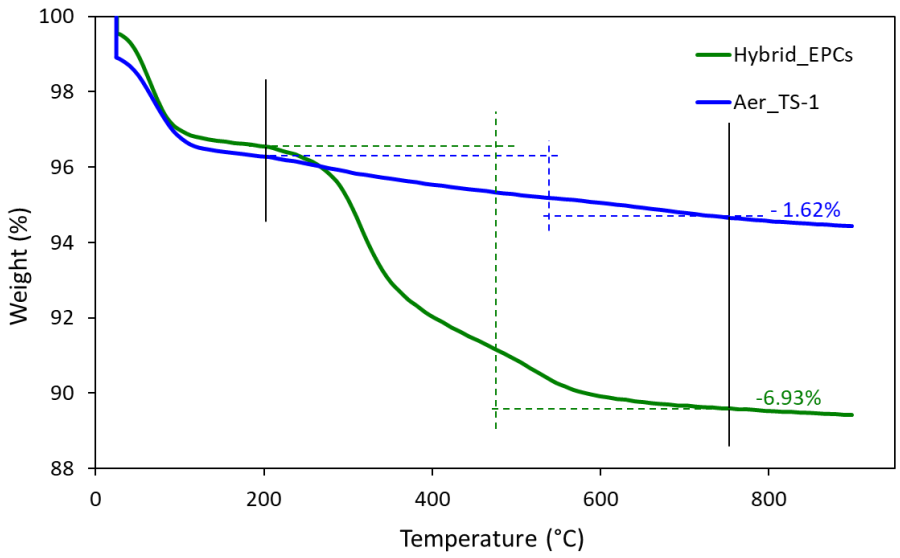

Figure S6. TGA of **Hybrid_EPCs** and **Aer_TS-1** used to determine the experimental loading of the organic content in the hybrid catalyst. The experimental loading of organic matter in **Hybrid_EPC** is calculated as followed:

$$Organic\ matter\ (\%) = \%\ Mass\ loss\ Hybrid_{EPCs_{200°C\ to\ 750°C}} - \%\ Mass\ loss\ Aer_{TS} - 1_{200°C\ to\ 750°C} = 5.31\%$$

The theoretical loading amounts to 50 mg.g^{-1} (45 mg of GOx and 5 mg of PAH).

Catalytic test

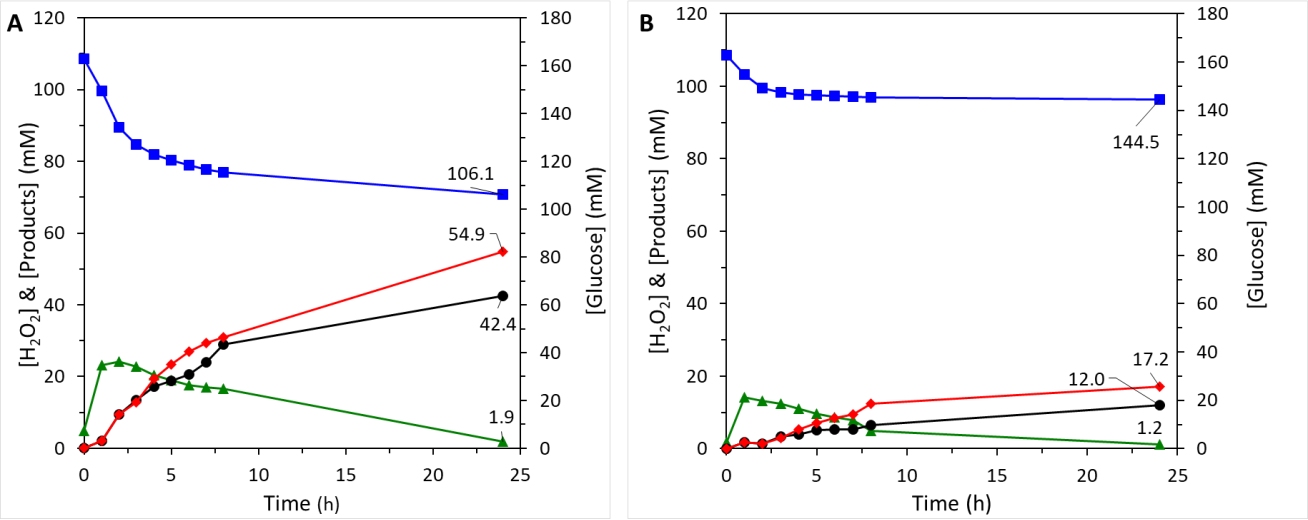

Figure S7. A) Repetition of the one-pot chemo enzymatic epoxidation of allyl alcohol with Hybrid_EPCs. Experimental conditions: T=45°C, [allyl alcohol] = 0.9 M, [Glucose] = 0.16 M, [Hybrid_EPCs] = 5g.L^{-1}. B) One-pot chemo enzymatic epoxidation of allyl alcohol with the two separate catalytic species Aer_TS-1 and the PAH-GOx complexes. Experimental conditions: T=45°C, [allyl alcohol] = 0.9 M, [Glucose] = 0.16 M, [Aer_TS-1] = 5g.L^{-1}, [GOx-PAH complexes] = 0.048 g.L^{-1}. ▲ Hydrogen peroxide, ● glycidol, ■ Glucose, ♦ Total (Glycidol+Glycerol).

The repetition of the cascade reaction test was performed with a new batch of hybrid catalyst following the same synthesis protocol. The performance was slightly decreased reaching an epoxide yield of 26% (compared to 30% during the first test) and a glucose conversion of 35%. The selectivity toward glycidol was improved with a value of 77%. The leaching of GOx was measured by Bradford assay and amounts to 7%.